Coordination-Induced Symmetry Breaking on Metal-Porphyrinic Framework Thin Films for Enhanced Nonlinear Optical Limiting

Yi-Bo Tian, Qiao-Hong Li, Zirui Wang, Zhi-Gang Gu,* and Jian Zhang

ABSTRACT: Structural asymmetry affecting the nonlinear optics (NLO) of metal−organic frameworks (MOFs) is very important in fundamentals and applications but is still a challenge. Herein we develop a series of indium-porphyrinic framework (InTCPP) thin films and provide the first study on the coordination-induced symmetry breaking on their third-order NLO. The continuous and oriented InTCPP(H_2) thin films were grown on quartz substrates and then postcoordinated with different cations (Fe^{2+} or $Fe^{3+}Cl^-$) in InTCPP(H_2) (named InTCPP(Fe^{2+}) and InTCPP($Fe^{3+}Cl^-$)). The third-order NLO results reveal the Fe^{2+} and $Fe^{3+}Cl^-$ coordinated InTCPP thin films have substantially enhanced NLO performance. Moreover, InTCPP($Fe^{3+}Cl^-$) thin films cause symmetry breaking of microstructures, resulting in a 3-fold increase in the nonlinear absorption coefficient (up to 6.35×10^{-6} m/W) compared to InTCPP(Fe^{2+}). This work not only develops a series of nonlinear optical MOF thin films but also provides new insight into symmetry breaking on MOFs for nonlinear optoelectronic applications.

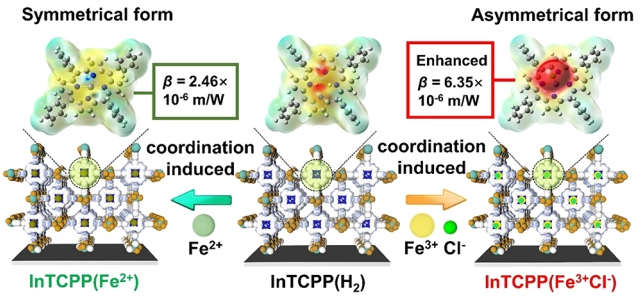

KEYWORDS: *Metal-porphyrinic frameworks, Thin films, Symmetry breaking, Coordination-induced, Nonlinear optical limiting*

With the fast advancement of laser technology and in-depth photon research, there is a growing interest in nonlinear optical (NLO) materials, which are the elementary cornerstones of future optoelectronics signal processing,[1,2] photonic circuits,[3] and optical switches.[4] The development of new NLO materials with excellent comprehensive properties is of great significance in numerous related disciplines.[5] Particularly, third-order NLO materials with high performance have been developed including organic molecules,[6,7] inorganic semiconductors,[8,9] carbon materials,[10,11] etc. Recently as a kind of inorganic−organic hybrid material, metal−organic frameworks (MOFs) have attracted remarkable attention in third-order NLO due to their tunable crystalline network and optoelectronic properties.[12−17] Especially, porphyrin-based MOFs (also known as metal-porphyrinic frameworks) are gradually attracting interest in NLO due to their unique and order charge model systems, which provide delocalized π-conjugation systems and have been verified to be excellent NLO materials in the potential applications of nonlinear optical limiting (OL), mode-locked lasers, etc.[18] To date, third-order NLO properties of such MOFs have been investigated by tuning the types of metal chelated ligands,[19] construction of interpenetrated networks,[20] encapsulation of guest species and thickness of MOFs films, as well as the electric field simulations.[21] These strategies can change the electronic structures of the materials, which further affect their NLO performances. As a special tunable strategy, breaking the structural symmetry of crystalline materials has the potential to enable strong anisotropic plasmon hybridization, and unusual phenomena such as plasmon-induced transparency, anti-Hermitian plasmonic antennas, and optical magnetism. On the basis of this idea, symmetry breaking will likely have a significant influence on the third-order NLO properties of MOFs but has never been studied.

For many optical devices, the ability to deposit homogeneous and continuous MOFs thin films on transparent substrates plays a crucial role, which can greatly extend the usage scenarios of MOFs.[22−24] Among the MOFs thin film preparation methods, liquid-phase epitaxial (LPE) and layer-by-layer (LBL) techniques have been developed to prepare monolithic, uniform, and compact MOF thin films on substrate surfaces, which are referred to as surface-coordinated MOF thin films (SURMOFs).[25,26] These films are particularly well-suited for third-order nonlinear optical (NLO) applications.[27,28] In this context, porphyrinic MOFs thin films made by the LPE LBL method with automatic facility have distinct benefits due to their low surface roughness, monolithic construction, robust adherence to the substrate surface,

Scheme 1. Schematic Diagram of the Fabrication Process of InTCPP SURMOFs[a]

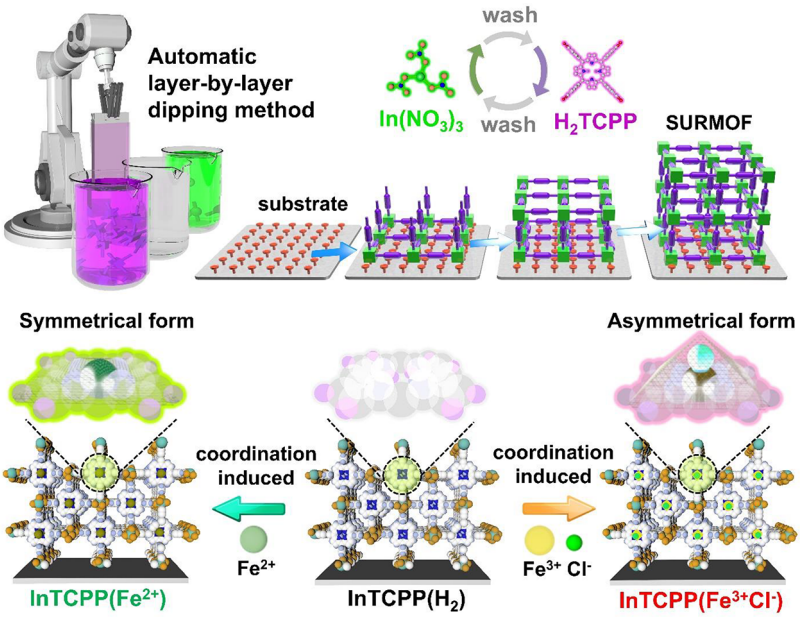

[a]Postcoordination process to get iron metallized InTCPP(Fe^{2+}) and InTCPP($Fe^{3+}Cl^{-}$) SURMOFs.

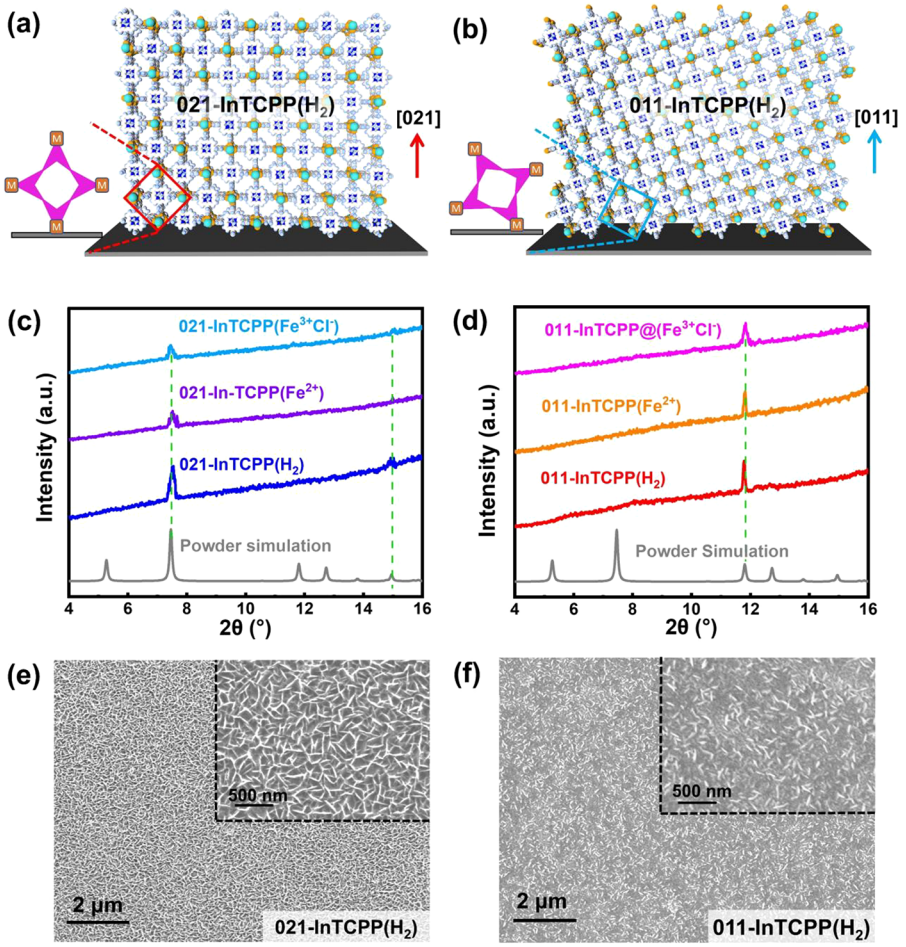

Figure 1. (a, b) Diagrammatic representation of the local orientation of [021] and [011] oriented InTCPP(H_2). (c, d) Out-of-plane XRD pattern of 021-InTCPP(H_2), 021-InTCPP(Fe^{2+}), 021-InTCPP($Fe^{3+}Cl^{-}$), 011-InTCPP(H_2), 011-InTCPP(Fe^{2+}), 011-InTCPP($Fe^{3+}Cl^{-}$), InTCPP(H_2), and powder simulation. Note: Using quartz substrates leads to the rising baselines in XRD data. (e, f) Top-view SEM images of 021- and 011-InTCPP(H_2) SURMOFs. All the SURMOFs samples were grown on quartz substrates.

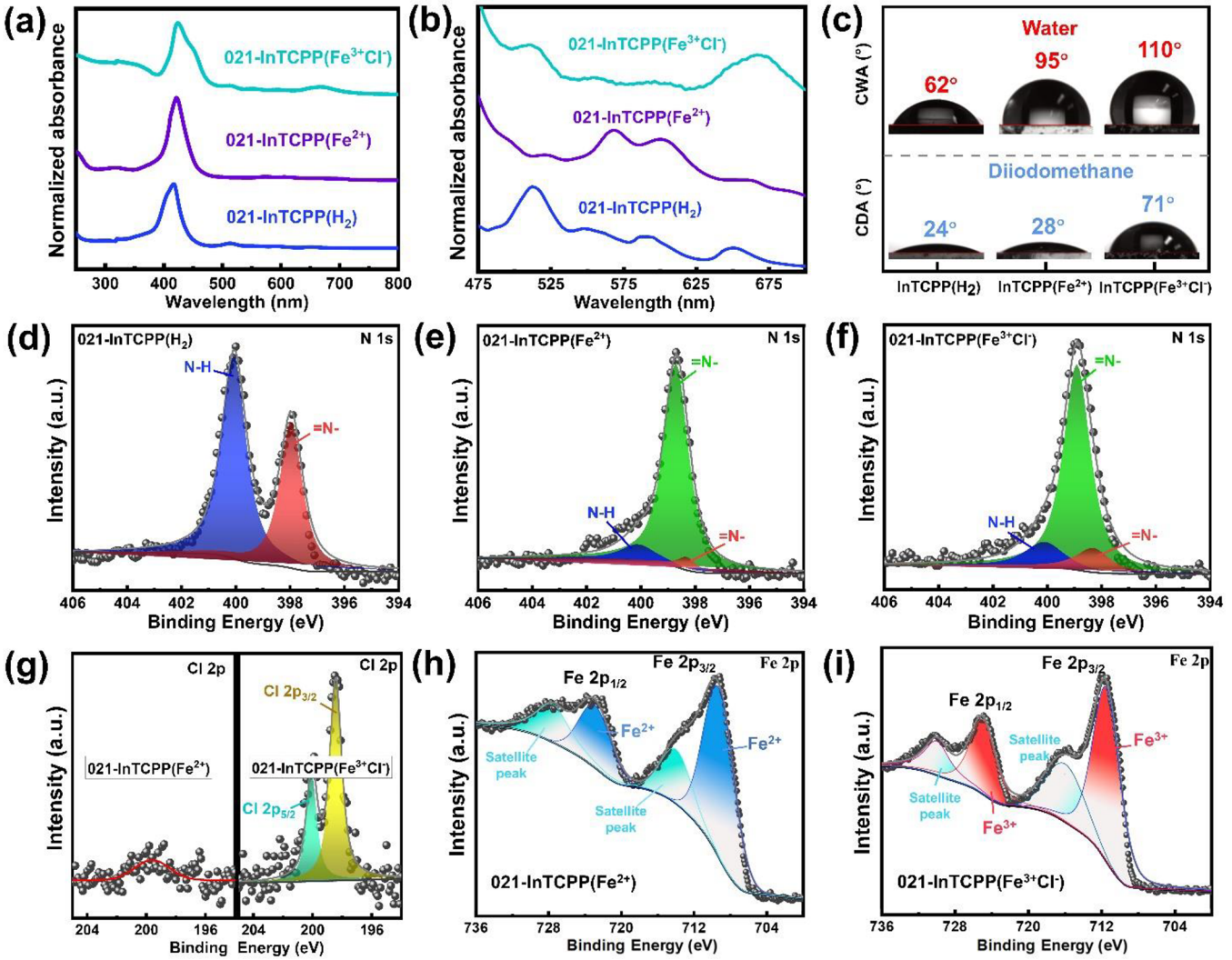

Figure 2. (a) UV−visible absorption spectra of 021-InTCPP SURMOF and postcoordinated SURMOFs. (b) Enlarged spectra of the Q-band wavelength, ranging from 475 to 700 nm. (c) The film contact angles of water and diiodomethane. (d) High-resolution XPS N 1s data of the 021-InTCPP(H_2) thin film. (e) N 1s XPS data with a high resolution for the 021-InTCPP(Fe^{2+}) thin film. (f) N 1s XPS data with a high resolution for the 021-InTCPP($Fe^{3+}Cl^-$) thin film. (g) Cl 1s XPS data with a high resolution for the thin film of metallized porphyrinic SURMOFs. (h) High-resolution XPS Fe 2p data of the 021-InTCPP(Fe^{2+}) thin film. (i) High-resolution XPS Fe 2p data of the 021-InTCPP($Fe^{3+}Cl^-$) thin film.

controlled orientation, and customizable thickness. Then, by using a postcoordinated process with different valent cations in the porphyrinic group of MOFs, the symmetry of the pristine porphyrinic MOFs structure can be broken. So, this is a good opportunity and a formidable challenge to explore the coordination-induced symmetry breaking on MOFs thin films for NLO properties.

Herein, we provide the first study on coordination-induced symmetry breaking MOFs thin films for third-order NLO study. In order to effectively control the variables, we synthesized a series of metalloporphyrinic MOF thin films with distinct symmetry and investigated the influence of the structural asymmetry of MOFs on the NLO property. Depending on the size, charge, and spin multiplicity, Fe^{2+} ions can fit into the center of the planar tetrapyrrolic ring system to form regular metalloporphyrins resulting in kinetically insert Fe^{2+} complexes. Comparatively, after the postcoordination procedure, the Fe^{3+} ion replaces the two protons and axially binds a Cl^- ion to establish a square-pyramidal-like structure, which can introduce an asymmetry motif in porphyrinic ligand and cause symmetry breaking compared to a planar structure. Based on the chemical coordination state of the center of the porphyrinic linker, our samples were categorized into three classes: InTCPP(H_2), InTCPP(Fe^{2+}), and In-TCPP($Fe^{3+}Cl^-$) SURMOFs. As described in our published work, the InTCPP(H_2) SURMOF assembly process was carried out.[29] Briefly, as shown in the upper part of Scheme 1, a functionalized quartz substrate was submerged into ethanolic solutions of $In(NO_3)_3$ and TCPP-(H_2) in turn under automatic control. The substrate was rinsed with ethanol between each step to remove unreacted attachments. By adjusting the concentration and the temperature of the precursor solution, InTCPP thin films with two alternative orientations of [021] and [011] can be fabricated (for details see the Supporting Information). Unless otherwise noted, the samples used in the experiments were grown on the surface of quartz substrates and manufactured using 30 cycles of LPE LBL procedures. InTCPP(Fe^{2+}) and In-TCPP-($Fe^{3+}Cl^-$) were made with different postcoordinations to get a pair of contrastive symmetries. As the cartoon displays in the

lower part of Scheme 1, metallized SURMOFs were produced by soaking pristine InTCPP(H_2) SURMOF into the Fe(II)/Fe(III) chloride DMF solution and heating in a nitrogen protected atmosphere to coordinate Fe ions with the porphyrinic ligand. Immersion in hot DMF solution of Fe salt is a widely adapted way to make metalloporphyrins. The structural deviation diminishes the symmetry of the porphyrinic plane,[30] and it provides an opportunity to further study the influence between the asymmetric electronic structure and enhanced NLO.

First, we did a systematic characterization for the SURMOF samples preparation. Figure 1a,b shows the schematic diagram of the local molecular arrangement of SURMOF in [021] and [011] orientations, in which the porphyrin planes are both perpendicular but a different angle to the substrate. The out-of-plane XRD patterns of 021-InTCPP(H_2) showed peaks at 7.5° and 15.0°, indicating the presence of a highly [021] orientation, which was achieved in a higher concentration and temperature (Figure 1c). As for XRD patterns of 011-InTCPP(H_2) shown in Figure 1d, its characteristic peaks appeared at 11.8°. The in-plane XRD pattern of the 021- and 011-InTCPP(H_2) shown in Figures S1 and S2 allow us to identify the extra peaks at 5.3° and 7.5° in the in-plane XRD data (Supporting Information) to confirm the crystal structure. These in-plane XRD peaks can evidence that InTCPP(H_2) thin films were successfully made at a mild temperature and concentration. The out-of-plane XRD peaks of metallized InTCPP(Fe^{2+}) and InTCPP($Fe^{3+}Cl^-$) were still present despite the film being submerged in hot DMF solution, indicating that the postcoordination step did not destroy the crystal structure. Figure S3 shows the XRD data for the nonoriented InTCPP films made by spin-coating powders on substrates.

Figure 1e,f shows the surface scanning electron microscopy (SEM) top-view of 021- and 011-InTCPP(H_2) SURMOFs grown on quartz substrates. The 021-InTCPP(H_2) thin film was composed of a dense and uniform arrangement of flakes that make up the surface of 011-InTCPP(H_2). It gets slightly rounder as a result of the postcoordination process in DMF solution, but its morphology does not change much from that of pristine SURMOF, as displayed in Figures S4 and S5. The cross-view SEM images of 021-InTCPP(H_2) and 011-InTCPP(H_2) are displayed in Figure S6. The thickness of the 021-InTCPP thin film was nearly 1 μm, and the 011-InTCPP thin film was about 600 nm. The transmission electron micrograph (TEM) of InTCPP was taken from the substrate after scraping and dispersing with ethanol (Figure S7). The crystal lattice seen with clarity has a lattice fringe distance of 1.8 nm, which coincides with the spacing of (021) planes.

The Q-band absorbance spectra of porphyrins was altered to a greater or lesser extent by the introduction of Fe^{2+} and $Fe^{3+}Cl^-$ modifications to the InTCPP(H_2) SURMOF. The porphyrinic ligand in In-TCPP(H_2) SURMOF reveals the vibronic structure of free-based porphyrin with four Q-band peaks in the area of 475−700 nm.[31] When a metal ion intercalates and replaces the central protons of porphyrin, the electronic structure of the porphyrinic group is altered, resulting in a change in the shape and strength of the Q-band.[32] The coordinations of Fe(II) and Fe(III) make the original four Q-band peaks reduced to two peaks. So in Figure 2a,b, there are two peaks at 563 and 597 nm in the UV−vis spectrum of 021-InTCPP(Fe^{2+}). And for 021-InTCPP-($Fe^{3+}Cl^-$), the UV−vis spectra introduced two peaks at 511 and 660 nm. The reduction in the number of Q-band peaks after post-treatment is a proof of the metallization.[33,34] Minor peaks in InTCPP(Fe^{2+}) and InTCPP($Fe^{3+}Cl^-$) is still observable, attributable to incomplete metallization of a small quantity of TCPP. However, this does not affect the ultimate outcome of the experimental results. A similar phenomena can also be reasonably explained in 011-InTCPP(Fe^{2+}) and 011-InTCPP($Fe^{3+}Cl^-$) represented by Figure S8. Analysis of the atom size reveals that Fe ions, a transition metal in period four, has a radius smaller than the size of the porphyrin core hole, and hence Fe^{2+} substitution has an insignificant effect on the geometrical coordination.[35] But to maintain charge equilibrium, Fe^{3+} ions need to axially connect to an anion to produce a square-pyramidal structure, resulting in an asymmetric structure. The porphyrinic structure in InTCPP($Fe^{3+}Cl^-$) is substantially disrupted because of the chemical modifications, leading to a symmetry breaking state. Since there is only molecular symmetry difference induced by postcoordination, InTCPP(Fe^{2+}) and InTCPP($Fe^{3+}Cl^-$) are a pair of strict control samples that allow us to investigate the effect of symmetry breaking on the nonlinear OL property of MOF thin films.

The surface composition and chemical surroundings of the thin film influence its surface energy, which quantifies the destruction of intermolecular bonds that happens when the surface is generated.[36] Reducing the surface energy can increase the MOF thin film's interface stability by increasing its water resistance. Utilizing a comparable contact angle analysis test, the effect of MOF coordinated on a quartz substrate was evaluated (the drop volumes of water and diiodomethane remained constant). By measuring the contact angle of water, it is revealed that the contact angle of water increases from the left to right side in Figure 2c. And due to the introduction of $Fe^{3+}Cl^-$, the contact angle of diiodomethane is dramatically increased. From the Young-Dupré equation ($\gamma_{sg} = \gamma_d + \gamma_p$), we calculated the surface energy of the 021-SURMOF and presented it in Figure S9. The MOF thin films with low surface energy tend to be more resistant to corrosion and can improve the longevity and durability. As the hydrophobic group Cl^- was introduced into InTCPP-($Fe^{3+}Cl^-$), the surface energy of the SURMOF decreases to minimum than InTCPP(H_2) and InTCPP(Fe^{2+}). This suggests that InTCPP($Fe^{3+}Cl^-$) SURMOF with symmetry breaking features exhibit the best stability, and it can be expected that this property will be beneficial for the application of nonlinear optical devices.

The binding energy of N 1s in X-ray photoelectron spectroscopy (XPS) can be used to distinguish between free base porphyrin and metalloporphyrin. The postcoordination process causes the free base proton to be replaced by metal ions (Fe^{2+} or Fe^{3+}), resulting in a different charge distribution among its N atoms. As shown in Figure 2d, the N−H and = N- of the free-base porphyrin units are thought to be responsible for the N 1s peaks observed at 399.9 and 398.2 eV for InTCPP(H_2) SURMOF. By replacing two hydrogen atoms with Fe(II) ions to form 021-InTCPP(Fe^{2+}), the four nitrogen of porphyrinic ligand become equivalent, and a single metallized nitrogen peak at 398.6 eV is generated, as shown in Figure 2e. Similar results can also be analyzed in the N 1s spectrum of the 021-InTCPP($Fe^{3+}Cl^-$) thin film (Figure 2f). The left portion of the Cl 2p spectrum in Figure 2g lacks the evident Cl element peaks, whereas the right portion of the

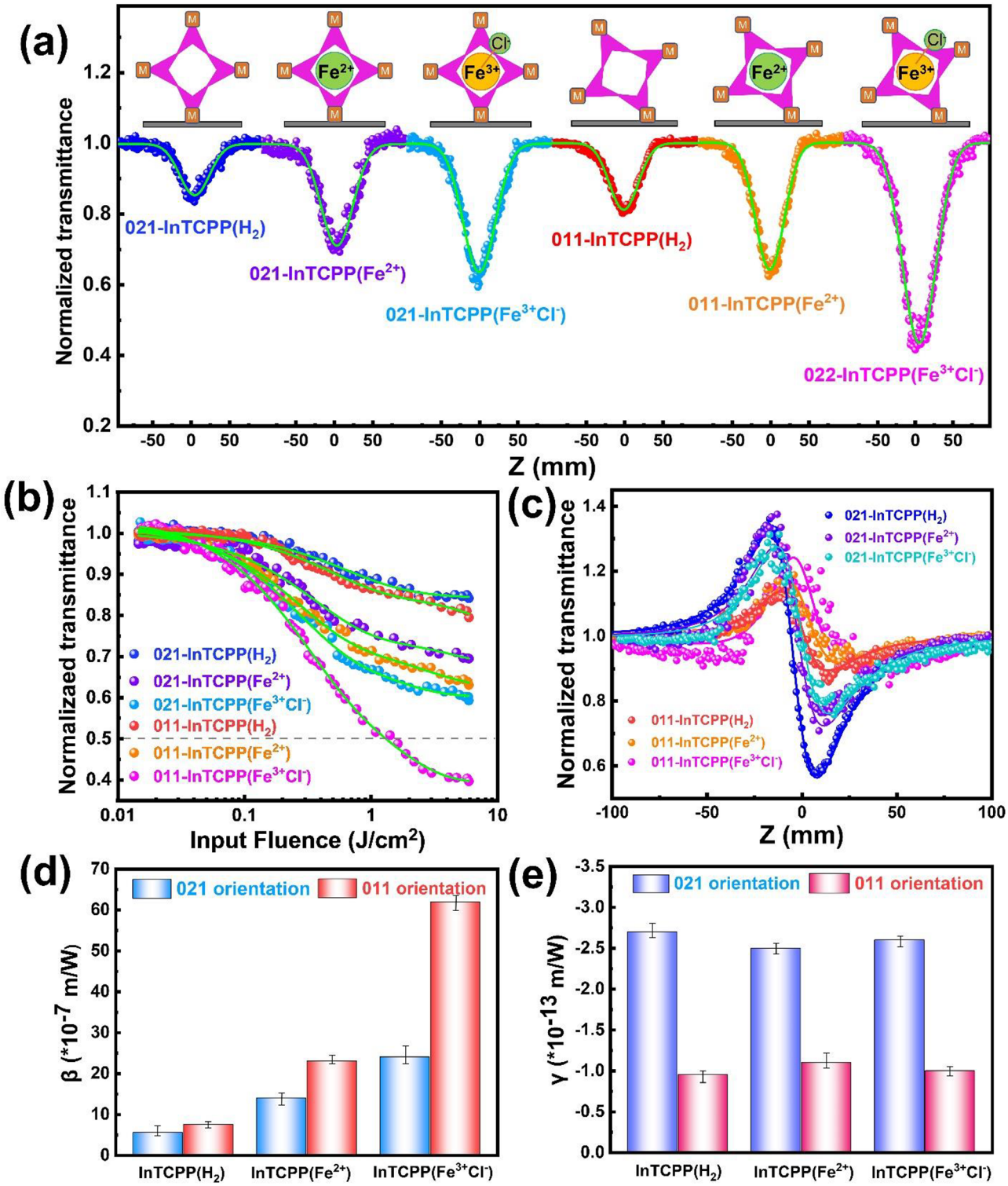

Figure 3. (a) Open-aperture plots of the series of InTCPP SURMOFs. (Inset scheme: "M" represents the metal unit In-Oxo node, the bottom gray is the substrate, the purple cross represents the porphyrin ligand, and the four sharp angles represent the four pairs of benzene and formic acid in TCPP molecule.) (b) Variation in the normalized transmittance as a function of input intensity. (c) Nonlinear refraction response of the series InTCPP SURMOF. (d) The third-order nonlinear absorption coefficient (β). (e) The calculated third-order polarizabilities (γ).

spectrum of 021-InTCPP($Fe^{3+}Cl^{-}$) contains the 2p orbital peaks that are characteristic of metallized chloride. The presence of Cl ions in InTCPP($Fe^{3+}Cl^{-}$) but not in InTCPP(Fe^{2+}) can also be a significant indicator of the valence state of the Fe ion at the center of the porphyrin ligand. Figure 2h,i illustrates the high-resolution XPS Fe 2p data for the metallized InTCPP thin film. The two peaks of the 2p orbital of Fe^{2+} have values of 409.5 and 422.9 eV, while the signal of Fe^{3+} exists at a higher energy of 411.2 and 424.8 eV. A series of XPS data including N 1s, Cl 2p, and Fe 2p for [011] orientation are presented in Figures S10–S15, which also

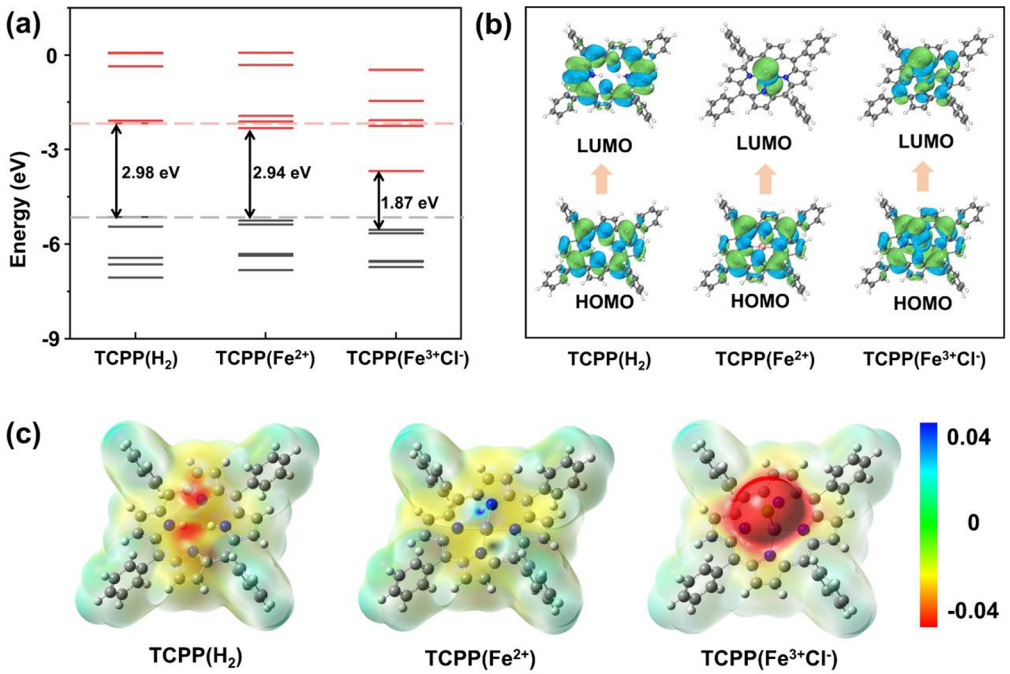

Figure 4. DFT calculations: (a) The HOMO−LUMO gaps of TCPP, TCPP(Fe^{2+}), and TCPP($Fe^{3+}Cl^{-}$), respectively. The smallest porphyrin unit cell is used for the calculations. (b) Some related frontier molecular orbitals of the TCPP units. (c) The electrostatic potential of different surface areas. (The blue part indicates a positive charge, and the red part indicates a negative charge.)

demonstrate the successful metallization by the postcoordination method.

The NLO performances of InTCPP SURMOFs were evaluated by a Z-scan technique with a 532 nm nanosecond laser at 70 μJ. The samples were mounted to a computer-controlled translation stage. The schematic diagram of the Z-scan device is shown in Figure S16. The SURMOFs of [021] and [011] orientations under 30 cycles are available in different thicknesses, with approximately 60% and 70% linear transmittance, respectively. XRD analysis of the (021) thin films before and after testing reveals no significant changes, indicating that laser illumination during the Z-scan testing did not cause notable damage to the SURMOF thin film (Figure S17). The coordination of Fe ions during the postcoordination process has no discernible effect on the transmission of SURMOF. The open-aperture Z-scan test for all films revealed varying degrees of typical reverse saturation absorption (RSA) responses (Figure 3a). The two kinds of orientations have similar performance trends. The minimum normalized transmittances (T_{min}) at $Z = 0$ for 021-InTCPP(H_2), 021-InTCPP(Fe^{2+}) and 021-InTCPP($Fe^{3+}Cl^{-}$) thin films were approximately 0.58, 0.69, and 0.82, respectively. The efficacy of third-order nonlinear protection is enhanced with a lower T_{min} for thin films of the same thickness. Under the premise that the RSA behavior can be modified by coordinating metal ions within the porphyrinic core, the symmetry breaking structure formed by Fe^{3+} and Cl ions insertion further greatly increases the optical limiting performance of the thin film. The 011-InTCPP SURMOFs exhibit a similar tendency, and the value of T_{min} decreases with the introduction of symmetric breaking. The results in Figure 3b showed that 011-InTCPP($Fe^{3+}Cl^{-}$) SURMOF exhibited the lowest normalized transmission (0.39) at the laser focal point. In addition, the uncoated quartz substrate served as the comparative reference and the open-aperture plots shown in Figure S17. The powder accumulation thin film made by a spin-coating approach is far less homogeneous, and although symmetry breaking and the introduction of Fe ions improve the T_{min} to 0.84, it is still far below the SURMOF produced by the LPE LBL method. Figure 4b depicts the correlation between the laser input fluence and the normalized transmittance of the thin films. It was observed that the normalized transmittance of InTCPP SURMOF remained almost steady at a low input fluence, but rapidly declined as the input fluence increased, with 011-InTCPP ($Fe^{3+}Cl^{-}$) exhibiting the sharpest rate of decrease. As illustrated in Figure 3c, each InTCPP thin film closed-aperture Z-scan curve exhibited a peak-to-valley shape that corresponded to a negative nonlinear refractive index and a characteristic self-defocusing propensity. The calculated third-order nonlinear absorption coefficient (β) values (Figure 3d) for 021-InTCPP ($Fe^{3+}Cl^{-}$) and 011-InTCPP ($Fe^{3+}Cl^{-}$) thin films were about 2.46×10^{-6} m/W and 6.35×10^{-6} m/W, respectively, which is a huge boost compared to the absorption coefficient value of 021-InTCPP (Fe^{2+}) and 011-InTCPP (Fe^{2+}). The third-order susceptibility ($\chi^{(3)}$) of 021-InTCPP ($Fe^{3+}Cl^{-}$) is calculated up to 3.54×10^{-7} esu. Such a dramatic increase in the nonlinear absorption coefficient implies a promising nonlinear optical limiting with the inserted Fe and Cl ions, indicating the occurrence of symmetry breaking from high symmetry (more ordered status) to low symmetry. There is no obvious and regular change of the third-order polarizabilities (γ) after being postcoordinated with different valent cations (Fe^{2+} and $Fe^{3+}Cl^{-}$) in porphyrinic frameworks, as represented in Figure 3e.

Theoretical studies based on DFT calculations were studied to understand the enhanced NLO performance in InTCPP SURMOFs. During the calculating procedure, the minimum TCPP units were adopted for further evaluation. The static second hyperpolarizabilities (γ) of the TCPP, TCPP(Fe^{2+}), and TCPP($Fe^{3+}Cl^{-}$) models were studied by the coupled

perturbed Kohn–Sham method.[37,38] From Figure 4a,b, the reduction of the HOMO–LUMO gap of TCPP(Fe^{2+}) and TCPP($Fe^{3+}Cl^{-}$) is because of the reduction of the lowest unoccupied molecular orbitals (LUMOs). Compared with nonmetallized TCPP(H_2), the decrease of LUMOs of coordination-induced metallized TCPP is due to the new orbitals introduced by Fe ions. Moreover, compared with TCPP(Fe^{2+}), the highest occupied molecular orbitals (HOMOs) of TCPP($Fe^{3+}Cl^{-}$) has an additional p orbital of Cl, and the LUMOs also have the porphyrinic ring and Cl ion participation in addition to the d orbital of Fe, which greatly reduces the bandgap and leads to an enhanced NLO performance. Figure 4c depicts the relative electrostatic potential of the series TCPP and shown in various colors (blue indicates positive charge and red indicates negative charge). The Fe^{3+} ion is a positive center, and the Cl^{-} ion as an electronegative group introduces a huge negative electrostatic potential in the axial direction (z direction) of the porphyrinic plane affecting the electric dipole moment of the whole structure. Table S1 presents the results of the electric dipole moment calculation. The introduction of Cl^{-} destroys the local symmetry of the porphyrinic structure and modifies its dipole moment. In numerical comparison, the TCPP(H_2) and TCPP(Fe^{2+}) are close to zero, while TCPP($Fe^{3+}Cl^{-}$) is extremely large, with the z direction being the primary contributor to the total value. These values indicate that the coordination-induced supermolecule is highly polarizable to the applied electric field. The larger dipole moments indicate that the molecule is chemically reactive, and the charge transfer could enhance the NLO activity. For TCPP(H_2), TCPP(Fe^{2+}), and TCPP($Fe^{3+}Cl^{-}$), the total magnitude was calculated to be 7.40×10^{-35}, 7.48×10^{-35}, and 1.11×10^{-33} esu, respectively. The calculated results show a gradually increasing trend when Fe ions are coordinated and form an asymmetric structure.

In summary, we investigated an unreported study on coordination-induced symmetry breaking affecting the nonlinear optical limiting of MOF thin films. We successfully fabricated two kinds of continuous and oriented InTCPP thin films by using a LPE LBL approach, and further metallized them into structural symmetrical InTCPP(Fe^{2+}) and asymmetrical InTCPP($Fe^{3+}Cl^{-}$) thin films. Due to the increased delocalization of the metalloporphyrins group, the Fe^{2+} and Fe^{3+} coordinated InTCPP (InTCPP(Fe^{2+}) and InTCPP-($Fe^{3+}Cl^{-}$)) thin films improved their nonlinear limiting effect and enhanced their third-order nonlinear absorption coefficient (β). More noteworthy is that symmetry breaking of the microstructure on InTCPP($Fe^{3+}Cl^{-}$) thin films resulted in a significant improvement of nonlinear optical limiting performance and about three times enhancement in nonlinear absorption coefficient (up to 6.35×10^{-6} m/W) than that of InTCPP(Fe^{2+}). In addition, the influence of coordination induced Fe^{2+}/$Fe^{3+}Cl^{-}$ units on the NLO performance of the presented MOFs is also confirmed by theoretical DFT calculation of electron–hole distributions and the electric dipole moment. These presented results not only offer new candidates for optical limiting materials but also extend to create a new understanding between microstructural symmetry breaking and nonlinear optics.

AUTHOR INFORMATION

Corresponding Author

Zhi-Gang Gu − *State Key Laboratory of Structural Chemistry, Fujian Institute of Research on the Structure of Matter, Chinese Academy of Sciences, 350002 Fuzhou, P. R. China;* orcid.org/0000-0001-6538-2917; Email: zggu@fjirsm.ac.cn

Authors

Yi-Bo Tian − *State Key Laboratory of Structural Chemistry, Fujian Institute of Research on the Structure of Matter, Chinese Academy of Sciences, 350002 Fuzhou, P. R. China; Institute of Functional Interfaces (IFG), Karlsruhe Institute of Technology (KIT), 76344 Eggenstein-Leopoldshafen, Germany*

Qiao-Hong Li − *State Key Laboratory of Structural Chemistry, Fujian Institute of Research on the Structure of Matter, Chinese Academy of Sciences, 350002 Fuzhou, P. R. China;* orcid.org/0000-0001-9286-3580

Zirui Wang − *State Key Laboratory of Structural Chemistry, Fujian Institute of Research on the Structure of Matter, Chinese Academy of Sciences, 350002 Fuzhou, P. R. China;* orcid.org/0000-0003-3094-0282

Jian Zhang − *State Key Laboratory of Structural Chemistry, Fujian Institute of Research on the Structure of Matter, Chinese Academy of Sciences, 350002 Fuzhou, P. R. China;* orcid.org/0000-0003-3373-9621

Author Contributions

The manuscript was written through contributions of all authors. All authors have given approval to the final version of the manuscript.

Notes

The authors declare no competing financial interest.

ACKNOWLEDGMENTS

This work was supported by the National Natural Science Foundation of China (21872148), Natural Science Foundation of Fujian Province (2022J06031), Youth Innovation Promotion Association of the Chinese Academy of Sciences (outstanding, Y2022081), and Fujian Science & Technology Innovation Laboratory for Optoelectronic Information of China (Grant No. 2021ZR131).

REFERENCES

(1) Wang, J.; Hu, X. Recent Advances in Graphene-Assisted Nonlinear Optical Signal Processing. *Journal of Nanotechnology* **2016**, *2016*, 7031913.

(2) Song, Y.; Chen, Y.; Jiang, X.; Liang, W.; Wang, K.; Liang, Z.; Ge, Y.; Zhang, F.; Wu, L.; Zheng, J.; Ji, J.; Zhang, H. Nonlinear Few-Layer Antimonene-Based All-Optical Signal Processing: Ultrafast Optical Switching and High-Speed Wavelength Conversion. *Adv. Opt. Mater.* **2018**, *6* (13), 1701287.

(3) Dalton, L. R.; Lao, D.; Olbricht, B. C.; Benight, S.; Bale, D. H.; Davies, J. A.; Ewy, T.; Hammond, S. R.; Sullivan, P. A. Theory-Inspired Development of New Nonlinear Optical Materials and Their Integration into Silicon Photonic Circuits and Devices. *Opt. Mater.* **2010**, *32* (6), 658–668.

(4) Castet, F.; Rodriguez, V.; Pozzo, J.-L.; Ducasse, L.; Plaquet, A.; Champagne, B. Design and Characterization of Molecular Nonlinear Optical Switches. *Acc. Chem. Res.* **2013**, *46* (11), 2656−2665.
(5) Luo, M.; Lin, C.; Lin, D.; Ye, N. Rational Design of the Metal-Free $KBe_2BO_3F_2$·(KBBF) Family Member $C(NH_2)_3SO_3F$ with Ultraviolet Optical Nonlinearity. *Angew. Chem., Int. Ed.* **2020**, *132* (37), 16112−16115.
(6) O'Flaherty, S. M.; Hold, S. V.; Cook, M. J.; Torres, T.; Chen, Y.; Hanack, M.; Blau, W. J. Molecular Engineering of Peripherally and Axially Modified Phthalocyanines for Optical Limiting and Nonlinear Optics. *Adv. Mater.* **2003**, *15* (1), 19−32.
(7) Mathews, S. J.; Kumar, S. C.; Giribabu, L.; Rao, S. V. Nonlinear Optical and Optical Limiting Properties of Phthalocyanines in Solution and Thin Films of PMMA at 633 nm Studied Using a Cw Laser. *Mater. Lett.* **2007**, *61* (22), 4426−4431.
(8) Dini, D.; Calvete, M. J.; Hanack, M. Nonlinear Optical Materials for the Smart Filtering of Optical Radiation. *Chem. Rev.* **2016**, *116* (22), 13043−13233.
(9) Li, R.; Wei, Z.; Zhao, H.; Yu, H.; Fang, X.; Fang, D.; Li, J.; He, T.; Chen, R.; Wang, X. Linear and Nonlinear Optical Characteristics of All-Inorganic Perovskite $CsPbBr_3$ Quantum Dots Modified by Hydrophobic Zeolites. *Nanoscale* **2018**, *10* (48), 22766−22774.
(10) Feng, M.; Zhan, H.; Chen, Y. Nonlinear Optical and Optical Limiting Properties of Graphene Families. *Appl. Phys. Lett.* **2010**, *96* (3), 033107.
(11) Liu, Z.; Zhang, X.; Yan, X.; Chen, Y.; Tian, J. Nonlinear Optical Properties of Graphene-Based Materials. *Sci. Bull.* **2012**, *57* (23), 2971−2982.
(12) Cook, T. R.; Zheng, Y.-R.; Stang, P. J. Metal-Organic Frameworks and Self-Assembled Supramolecular Coordination Complexes: Comparing and Contrasting the Design, Synthesis, and Functionality of Metal-Organic Materials. *Chem. Rev.* **2013**, *113* (1), 734−777.
(13) Li, B.; Wen, H.-M.; Cui, Y.; Zhou, W.; Qian, G.; Chen, B. Emerging Multifunctional Metal-Organic Framework Materials. *Adv. Mater.* **2016**, *28* (40), 8819−8860.
(14) Farrusseng, D.; Aguado, S.; Pinel, C. Metal-Organic Frameworks: Opportunities for Catalysis. *Angew. Chem., Int. Ed.* **2009**, *48* (41), 7502−7513.
(15) Zhang, R.; Wang, B.; Wang, F.; Chen, S.-M.; Zhang, J. Syntheses of Ferrocene-Functionalized Indium-Based Metal-Organic Frameworks for Third Order Nonlinear Optical Application. *Inorg. Chem. Front.* **2022**, *10* (1), 201−210.
(16) Jiang, X.; Zhang, L.; Liu, S.; Zhang, Y.; He, Z.; Li, W.; Zhang, F.; Shi, Y.; Lü, W.; Li, Y.; Wen, Q.; Li, J.; Feng, J.; Ruan, S.; Zeng, Y.-J.; Zhu, X.; Lu, Y.; Zhang, H. Ultrathin Metal-Organic Framework: An Emerging Broadband Nonlinear Optical Material for Ultrafast Photonics. *Adv. Opt. Mater.* **2018**, *6* (16), 1800561.
(17) Abazari, R.; Yazdani, E.; Nadafan, M.; Kirillov, A. M.; Gao, J.; Slawin, A. M.; Carpenter-Warren, C. L. Third-Order Nonlinear Optical Behavior of an Amide-Tricarboxylate Zinc (II) Metal-Organic Framework with Two-Fold 3D+ 3D Interpenetration. *Inorg. Chem.* **2021**, *60* (13), 9700−9708.
(18) Shi, R.; Han, X.; Xu, J.; Bu, X.-H. Crystalline Porous Materials for Nonlinear Optics. *Small* **2021**, *17* (22), 2006416.
(19) Li, D.-J.; Li, Q.-h.; Gu, Z.-G.; Zhang, J. Oriented Assembly of 2d Metal-Pyridylporphyrinic Framework Films for Giant Nonlinear Optical Limiting. *Nano Lett.* **2021**, *21* (23), 10012−10018.
(20) Li, D.-J.; Li, Q.-h.; Wang, Z.-R.; Ma, Z.-Z.; Gu, Z.-G.; Zhang, J. Interpenetrated Metal-Porphyrinic Framework for Enhanced Nonlinear Optical Limiting. *J. Am. Chem. Soc.* **2021**, *143* (41), 17162−17169.
(21) Li, D.-J.; Gu, Z.-G.; Zhang, J. Auto-Controlled Fabrication of a Metal-Porphyrin Framework Thin Film with Tunable Optical Limiting Effects. *Chem. Sci.* **2020**, *11* (7), 1935−1942.
(22) Shekhah, O.; Liu, J.; Fischer, R.; Wöll, C. MOF Thin Films: Existing and Future Applications. *Chem. Soc. Rev.* **2011**, *40* (2), 1081−1106.
(23) Gu, Z.-G.; Zhang, J. Epitaxial Growth and Applications of Oriented Metal-Organic Framework Thin Films. *Coord. Chem. Rev.* **2019**, *378*, 513−532.
(24) Li, Z.; Liu, J.; Feng, L.; Liu, X.; Xu, Y.; Zhou, F.; Liu, W. Coupling Tandem MOFs in Metal-Insulator-Metal Resonator Advanced Chemo-Sieving Sensing. *Nano Today* **2023**, *48*, 101726.
(25) Li, Z.; Liu, J.; Feng, L.; Pan, Y.; Tang, J.; Li, H.; Cheng, G.; Li, Z.; Shi, J.; Xu, Y.; Liu, W. Monolithic MOF-Based Metal-Insulator-Metal Resonator for Filtering and Sensing. *Nano Lett.* **2023**, *23*, 637−644.
(26) Li, Z.; Liu, J.; Wu, H.; Tang, J.; Li, Z.; Xu, Y.; Zhou, F.; Liu, W. Photonic Crystals Constructed by Isostructural Metal-Organic Framework Films. *Nano Research* **2023**, DOI: 10.1007/s12274-023-5505-5.
(27) Gu, C.; Zhang, H.; You, P.; Zhang, Q.; Luo, G.; Shen, Q.; Wang, Z.; Hu, J. Giant and Multistage Nonlinear Optical Response in Porphyrin-Based Surface-Supported Metal-Organic Framework Nanofilms. *Nano Lett.* **2019**, *19* (12), 9095−9101.
(28) Ma, Z.-Z.; Li, Q.-H.; Wang, Z.; Gu, Z.-G.; Zhang, J. Electrically Regulating Nonlinear Optical Limiting of Metal-Organic Framework Film. *Nat. Commun.* **2022**, *13*, 6347.
(29) Tian, Y.-B.; Vankova, N.; Weidler, P.; Kuc, A.; Heine, T.; Wöll, C.; Gu, Z.-G.; Zhang, J. Oriented Growth of In-Oxo Chain Based Metal-Porphyrin Framework Thin Film for High-Sensitive Photodetector. *Adv. Sci.* **2021**, *8* (14), 2100548.
(30) Kingsbury, C. J.; Senge, M. O. The Shape of Porphyrins. *Coord. Chem. Rev.* **2021**, *431*, 213760.
(31) Stradomska, A.; Knoester, J. Shape of the *Q* Band in the Absorption Spectra of Porphyrin Nanotubes: Vibronic Coupling or Exciton Effects? *J. Chem. Phys.* **2010**, *133* (9), 094701.
(32) Liu, J.; Zhou, W.; Liu, J.; Howard, I.; Kilibarda, G.; Schlabach, S.; Coupry, D.; Addicoat, M.; Yoneda, S.; Tsutsui, Y.; Sakurai, T.; Seki, S.; Wang, Z.; Lindemann, P.; Redel, E.; Heine, T.; Wöll, C. Photoinduced Charge-Carrier Generation in Epitaxial Mof Thin Films: High Efficiency as a Result of an Indirect Electronic Band Gap? *Angew. Chem., Int. Ed.* **2015**, *54* (25), 7441−7445.
(33) Humphrey, J.; Kuciauskas, D. Charge-Transfer States Determine Iron Porphyrin Film Third-Order Nonlinear Optical Properties in the near-Ir Spectral Region. *J. Phys. Chem. B* **2004**, *108* (32), 12016−12023.
(34) Chen, J.; Gao, Y.; Ma, Q.; Hu, X.; Xu, Y.; Lu, X. Turn-Off Fluorescence Sensor Based on the 5, 10, 15, 20-(4-Sulphonatophenyl) Porphyrin ($TPPS_4$)-Fe^{2+} System: Detecting of Hydrogen Peroxide (H_2O_2) and Glucose in the Actual Sample. *Sens. Actuators B Chem.* **2018**, *268*, 270−277.
(35) Hashimoto, T.; Choe, Y.-K.; Nakano, H.; Hirao, K. Theoretical Study of the Q and B Bands of Free-Base, Magnesium, and Zinc Porphyrins, and Their Derivatives. *J. Phys. Chem. A* **1999**, *103* (12), 1894−1904.
(36) Zhang, F.; Mohammadi, E.; Luo, X.; Strzalka, J.; Mei, J.; Diao, Y. Critical Role of Surface Energy in Guiding Crystallization of Solution-Coated Conjugated Polymer Thin Films. *Langmuir* **2018**, *34* (3), 1109−1122.
(37) Lescos, L.; Sitkiewicz, S. P.; Beaujean, P.; Blanchard-Desce, M.; Champagne, B.; Matito, E.; Castet, F. Performance of Dft Functionals for Calculating the Second-Order Nonlinear Optical Properties of Dipolar Merocyanines. *Phys. Chem. Chem. Phys.* **2020**, *22* (29), 16579−16594.
(38) Bhunia, M. K.; Melissen, S.; Parida, M. R.; Sarawade, P.; Basset, J.-M.; Anjum, D. H.; Mohammed, O. F.; Sautet, P.; Le Bahers, T.; Takanabe, K. Dendritic Tip-on Polytriazine-Based Carbon Nitride Photocatalyst with High Hydrogen Evolution Activity. *Chem. Mater.* **2015**, *27* (24), 8237−8247.